SCIENTIFIC REPORTS

OPEN

SUBJECT AREAS:
ELECTRONIC AND SPINTRONIC DEVICES
ORGANIC LEDS
POLYMERS

Received
9 October 2013

Accepted
27 December 2013

Published
28 January 2014

Correspondence and requests for materials should be addressed to J.-J.K. (jjkim@snu.ac.kr)

Formation of perfect ohmic contact at indium tin oxide/*N*,*N*′-di(naphthalene-1-yl)-*N*,*N*′-diphenyl-benzidine interface using ReO_3

Seung-Jun Yoo[1], Jung-Hung Chang[2], Jeong-Hwan Lee[1], Chang-Ki Moon[3], Chih-I Wu[2] & Jang-Joo Kim[1,3]

[1]WCU Hybrid Materials Program, Department of Materials Science and Engineering and the Center for Organic Light-Emitting Diodes, Seoul National University, Seoul 151-744, South Korea, [2]Graduated Institute of Photonics and Optoelectronics and Department of Electrical Engineering, National Taiwan University, Taipei 106, Taiwan, [3]Department of Materials Science and Engineering, Seoul National University, Seoul 151-744, South Korea.

A perfect ohmic contact is formed at the interface of indium tin oxide (ITO) and *N*,*N*′-di(naphthalene-1-yl)-*N*,*N*′-diphenyl-benzidine (NPB) using ReO_3 as the interfacial layer. The hole injection efficiency is close to 100% at the interface, which is much higher than those for interfacial layers of 1,4,5,8,9,11-hexaazatripheylene hexacarbonitrile (HAT-CN) and MoO_3. Interestingly, the ReO_3 and MoO_3 interfacial layers result in the same hole injection barrier, ≈0.4 eV, to NPB, indicating that the Fermi level is pinned to the NPB polaron energy level. However, a significant difference is observed in the generated charge density in the NPB layer near the interfacial layer/NPB interface, indicating that charge generation at the interface plays an important role in forming the ohmic contact.

The formation of ohmic contacts at metal/organic semiconductor (M/OS) interfaces or indium tin oxide (ITO)/OS interfaces is one of the most important techniques for removing parasitic resistance in organic semiconductor devices. Several methods have been used to form ohmic contacts at M/OS or ITO/OS interfaces, including surface modification of ITO[1,2], heavy doping of organic semiconductors with *p*- and *n*-dopants[3–8], and insertion of an interfacial layer possessing a deep Fermi level between the metal and organic semiconductor layers[9–14]. Among these, insertion of a thin interfacial layer is widely used because it is simple and effective.

Despite the wide use of interfacial layers, perfect ohmic contacts between ITO and organic hole-transporting layers have rarely been reported; ohmic contacts are evaluated using the charge injection efficiency (η_{INJ}), defined by the following equation[15]:

$$\eta_{INJ} = \frac{J_{INJ}}{J_{BULK}},$$

where J_{INJ} is the injection-limited current density, which is the measured steady-state current density of a single carrier device, and J_{BULK} is the bulk-limited current density, which is the theoretical maximum current density that can flow through the organic semiconductors. According to the above definition of charge injection efficiency, the perfect ohmic contact supplies the organic semiconductor with a current density equal to J_{BULK} and has a charge injection efficiency of 100%. Recently, the charge injection efficiencies at various contacts have been reported; examples include the insertion of thin layers of WO_x, V_2O_x, and MoO_3, with η_{INJ} values of 20–40%[9], 5–8%[9], and ≈5%[10], respectively, for hole injection from ITO to *N*,*N*′-di(naphthalene-1-yl)-*N*,*N*′-diphenyl-benzidine (NPB). The formation of a perfect ohmic contact as the top contact of NPB/1,4,5,8,9,11-hexaazatripheylene hexacarbonitrile (HAT-CN)/Au has been reported, but the hole injection efficiency was only about 30% at the bottom contact of ITO/HAT-CN/NPB[10]. The injection efficiencies of ITO/hole-transporting organic semiconductors are as yet far from perfect ohmic contacts.

In this paper, we report that perfect ohmic contacts can be formed between ITO and NPB layers using ReO_3[7,16] as the interfacial layer. Ultraviolet photoelectron spectroscopy (UPS), X-ray photoelectron spectroscopy (XPS), and photoluminescence (PL) measurements indicated that energy barrier lowering and charge generation in the

NPB layer near the interfacial layer/NPB interface with an ReO_3 layer result in formation of a perfect ohmic contact.

Results

Hole injection efficiency. Hole-only devices with the structure ITO/high EA material (1 nm)/NPB (1,000 nm)/high EA material (1 nm)/Ag (70 nm) were used to investigate the hole injection efficiency, where EA is the electron affinity. Various high EA materials, i.e. HAT-CN, MoO_3, and ReO_3, were used to investigate the effectiveness of the interlayer in the enhancement of the hole injection properties. A thick NPB layer (1,000 nm) was used to reduce the effect of the built-in field, and thin interlayers (1 nm) were used at both contacts in the hole-only devices to minimize the effect of the bulk resistance of the high EA layers. Fig. 1a and 1b show the current density–average applied electric field (*J–F*) characteristics of hole-only devices with high EA materials as the interlayer. The *J–F* characteristics of a hole-only device with no interlayer are also displayed in the figures for comparison. The current densities were significantly enhanced by inserting interlayers compared with those of the device without an interlayer. Among the interlayers, ReO_3 gave the highest current density, followed by MoO_3 and HAT-CN. The current density with an ReO_3 interlayer was about one order of magnitude larger than that with an MoO_3 interlayer.

For calculation of the hole injection efficiencies from the *J–F* characteristics, we need to obtain J_{BULK} using equation (1), which can be expressed using the field-dependent space-charge-limited current (SCLC) as follows[17,18]:

$$J_{\mathrm{BULK}} = J_{\mathrm{PF\text{-}SCLC}} = \frac{9}{8}\varepsilon_0\varepsilon_r\mu_0 \exp\left(0.89\beta\sqrt{F}\right)\frac{F^2}{L}, \qquad (1)$$

where ε_r is the relative dielectric constant, ε_0 is the permittivity of a vacuum, μ_0 is the zero-field mobility, β is the Poole–Frenkel (PF) coefficient, F is the average applied electric field, and L is the thickness of the organic semiconductor layer. The $J_{\mathrm{PF\text{-}SCLC}}$ value was calculated using μ_0 and β measured using the time-of-flight method (Supplementary Fig. S1a, S1b) and known values of F and L. We used a dielectric constant of 3. The experimentally obtained μ_0 and β values were 2.85×10^{-4} $cm^2/(V\ s)$ and 1.27×10^{-3} $(V/cm)^{1/2}$, respectively. The values are very close to the reported values for NPB[19,20]. The PF-type SCL current density is shown in Fig. 1a and 1b as a solid line. The $J_{\mathrm{PF\text{-}SCLC}}$ is very close to the *J–F* characteristics of a hole-only device with an ReO_3 interlayer.

The hole injection efficiencies of hole-only devices with various high EA materials, extracted from Fig. 1a and 1b, are plotted in Fig. 1c as a function of the average applied electric field. The hole injection efficiency is almost 100% with an ReO_3 interlayer, indicating that a perfect ohmic contact is formed in the device using this interlayer. To the best of our knowledge, this is the highest hole injection efficiency reported to date for an ITO/NPB contact. In contrast, the HAT-CN and MoO_3 interlayers gave much lower hole injection efficiencies, 2.3% and 8.9%, respectively, at 150 kV/cm.

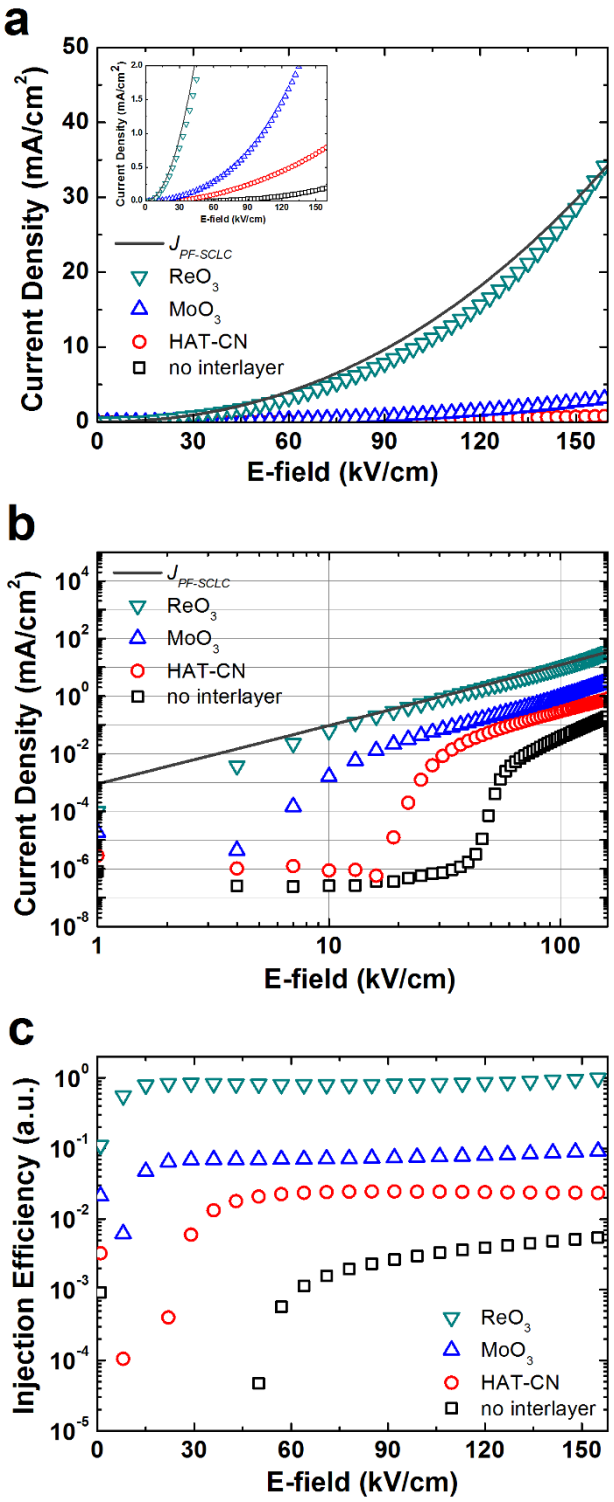

Figure 1 | *J–F* characteristics and hole injection efficiencies of hole-only devices. (a) *J–F* characteristics in linear scale of hole-only devices with various high EA materials as the interlayer or without an interlayer. The current density designates the absolute magnitude. The open symbols represent measured values and the solid line represents calculated field-dependent SCLCs. *Inset*: close-up view of the same *J–F* data. (b) Same *J–F* data on logarithmic axes. (c) Hole injection efficiencies of hole-only devices as a function of average applied electric field, obtained from the equation $\eta_{\mathrm{INJ}} = J_{\mathrm{INJ}}/J_{\mathrm{BULK}}$.

Energy level alignment based on UPS measurements. In order to understand the hole injection properties, the energy level alignments at ITO/high EA materials/NPB interfaces were investigated using UPS measurements. Fig. S2 shows the UPS (He Iα, 21.2 eV) spectra of the samples with incremental deposition of NPB on ITO/high EA material (1 nm) substrates. The normalized secondary electron cut-off regions are displayed in the left panels, and close-up views of the valence band regions are displayed in the right panels. All binding energies are referenced to the ITO Fermi level. The initial cut-off position of ITO, with a work function (W_F) of 4.22–4.40 eV, moves toward the lower binding energy side by 0.52 eV (HAT-CN), 1.61 eV (MoO_3), and 1.80 eV (ReO_3) after deposition of a 1 nm thick interlayer. The work functions of the 1 nm thick interlayer are 4.86 eV (HAT-CN), 6.01 eV (MoO_3), and 6.02 eV (ReO_3). These values are much smaller than the work functions of the bulk high EA materials. The work function of a

20 nm thick HAT-CN layer is 5.52 eV and that of a bulk MoO_3 layer is 6.9 eV, as reported in the literature[21,22]. The work function of a bulk ReO_3 layer is 6.75 eV, obtained by UPS measurements of a 10 nm thick ReO_3 layer deposited on a sputtered Au substrate, as shown in Fig. S3. These results might indicate that the 1 nm thick interlayers form islands rather than continuous films. Deposition of an NPB layer of thickness 6–8 nm on an ITO/high EA material (1 nm) substrate results in large vacuum level shifts toward higher binding energies of 0.37 eV (HAT-CN/NPB), 1.46 eV (MoO_3/NPB), and 1.32 eV (ReO_3/NPB). These large negative vacuum level shifts are generated by the combined effect of the interface dipole resulting from electron transfer from NPB to the high EA materials and energy level bending[23]. The highest occupied molecular orbital (HOMO) onset of NPB on a high EA material layer increased gradually with increasing NPB thickness, because interfacial *p*-type doping was generated at the high EA material/NPB interface. The values of the vacuum level shift and HOMO onset shift for various thin high EA material layers as a function of the thickness of the NPB layer are summarized in Fig. 2.

Estimation of the hole injection barrier, which is defined by the energy difference between the Fermi level of the electrodes and the HOMO level of the organic layers, from the UPS spectra requires separation of the interfacial dipole effect and energy level bending in the vacuum level shifts. When the NPB comes into contact with the high EA material without rearrangement of the electric charge, the organic layer is in the potential of the surface dipole of the high EA material layer in an extremely narrow interfacial gap. However, for an interface with a thick organic layer, band bending, which arises by redistribution of charges between the high EA material layer and the NPB layer, should also be considered, because the work functions of the high EA material layer and NPB are different[23]. In the band-bending region, the vacuum level shift is parallel to that of NPB HOMO onset. Based on the above discussion, the hole injection barrier is defined by the NPB HOMO onset at around 0.8 nm, since the HOMO onset shift of the NPB film does not change much in the first few nanometres compared with the vacuum level shift. The hole injection barriers are 0.86 eV at HAT-CN/NPB, 0.41 eV at MoO_3/NPB, and 0.38 eV at ReO_3/NPB, in the vicinity of the interfacial region. These hole injection barriers are much smaller than that at the ITO/NPB interface (1.64 eV)[24]. Fig. 3 shows the energy level alignment diagram for the ITO/high EA materials/NPB structure.

Recently, the energy alignment of organic semiconductors on transition metal oxides has been expressed by a simple plot, as follows[22]:

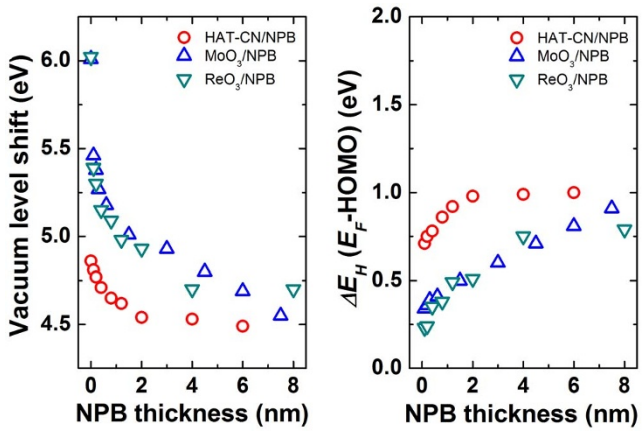

Figure 2 | Summary of values of vacuum level shift (*left panel*) and HOMO onset shift (*right panel*) on various thin high EA material layers, as a function of NPB film thickness.

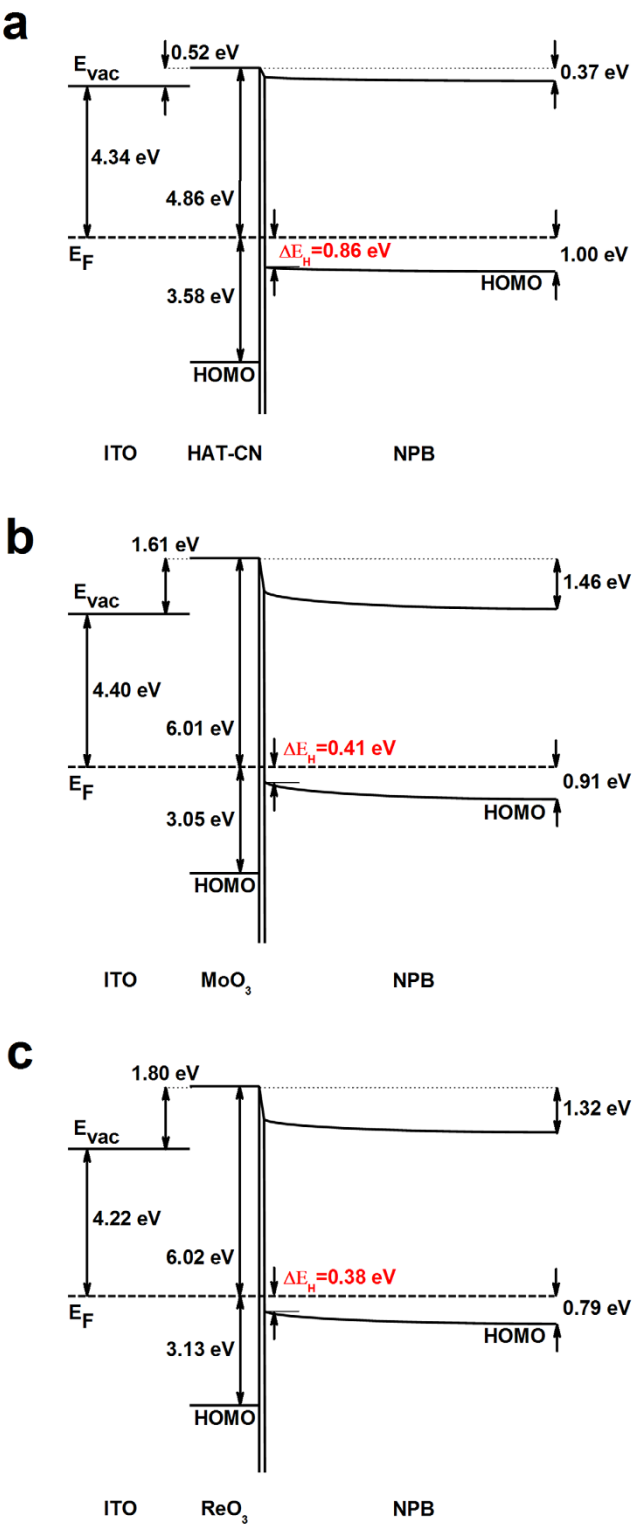

Figure 3 | Energy level alignment diagram for ITO/high EA materials/NPB structure. (a) ITO/HAT-CN/NPB, (b) ITO/MoO_3/NPB, and (c) ITO/ReO_3/NPB.

$$\Delta E_{\mathrm{H}} \sim \left(IE_{\mathrm{org}} - \Phi\right) + 0.3 \rightarrow \left(\Phi < IE_{\mathrm{org}}\right)$$
$$\Delta E_{\mathrm{H}} \sim 0.3 \rightarrow \left(\Phi > IE_{\mathrm{org}}\right) \quad (2)$$

where ΔE_{H} is the hole injection barrier, IE_{org} is the ionization energy of the organic semiconductor, and Φ is the work function of the substrate. Fig. 4 shows the hole injection barriers (open symbol) of

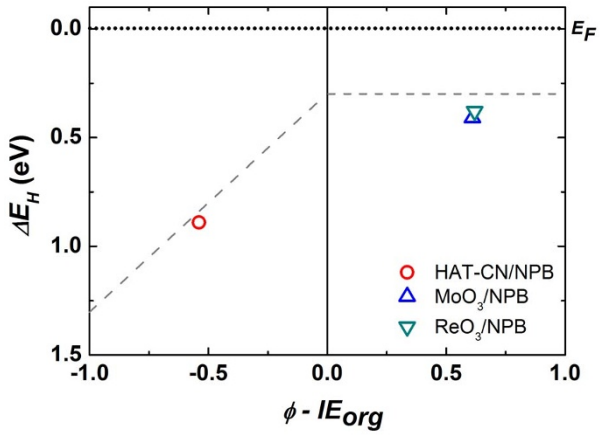

Figure 4 | Hole injection barriers of our systems as a function of energy differences between work functions of 1 nm thick high EA materials and ionization energy of NPB. The open symbols represent measured values from UPS measurements and the dashed line represents the universal energy alignment of organic semiconductors on transition metal oxides, reported by M. T. Greiner *et al.*

our systems, and equation (2) (dashed line), as a function of the energy differences between the work functions of 1 nm thick high EA materials and the ionization energy of NPB. The trend in the hole injection barrier is in good agreement with equation (2), even though HAT-CN is not a transition metal oxide but an organic semiconductor. The hole injection barriers were pinned at ≈0.4 eV with the MoO_3 and ReO_3 interlayers, whereas the hole injection barrier increased to 0.86 eV with the HAT-CN interlayer. The hole injection barriers with the MoO_3 and ReO_3 interlayers were consistent with the polaron energy of NPB, which is defined as an energy difference between the ionization energy of NPB by 5.35 eV and the positive integer charge-transfer state (E_{ICT+}) by 4.9 eV, indicating that the Fermi level was pinned to the E_{ICT+} of NPB[25,26].

Degree of charge generation at high EA materials/NPB interfaces. The hole injection barrier with a HAT-CN interlayer is much higher than those with MoO_3 and ReO_3 interlayers, consistent with the hole injection efficiency for the *J–F* characteristics. However, the hole injection properties with the ReO_3 interlayer are superior to those with the MoO_3 interlayer, although the hole injection barrier is almost the same, i.e. ≈0.4 eV. Also, the formation of a perfect ohmic contact using the ReO_3 interlayer cannot be explained, based on the measured hole injection barrier (0.38 eV), by *J–F* simulation using the drift-diffusion model, which results in a potential drop at the ITO/NPB contact of 0.38 eV[13]. There must be another factor influencing the injection characteristics of the interlayers; this was identified using XPS. Fig. 5 shows the XPS spectra of MoO_3 films for the Mo 3d core levels (Fig. 5a) and of ReO_3 films for the Re 4f core levels (Fig. 5b). The spectrum of the 1 nm thick MoO_3 film shows not only a single Mo $3d_{3/2}$ and $3d_{5/2}$ doublet, but also significant pair of shoulder peaks. The binding energies of the Mo $3d_{3/2}$ and Mo $3d_{5/2}$ doublet are 235.8 eV and 232.8 eV, respectively; these values are close to the reported values[27]. The pair of shoulder peaks is located at 234.7 eV and 231.3 eV, respectively, by Gaussian curve fitting as shown in Fig. S4a. These shoulder peaks are reduced forms of Mo such as Mo^V species[28,29] which can be generated by oxygen deficiencies during the thermal evaporation process. The ratio between Mo^{VI} and Mo^V is 67% : 33% in the 1 nm thick MoO_3 film. The oxygen deficiencies are the origins of gap states which are generated close to the Fermi level[29,30], as shown in our UPS spectra in Fig. S2. The portion of the doublet at the lower binding energy increases after deposition of NPB on the MoO_3 film, indicating the generation of Mo^V species. The ratio

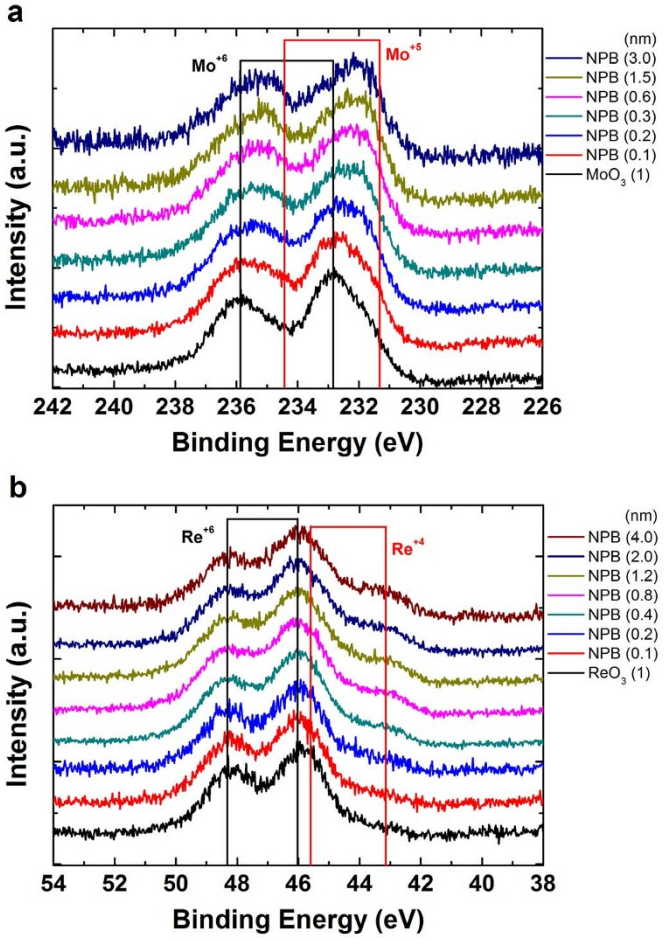

Figure 5 | XPS spectra of Mo 3d core levels of MoO_3 films and Re 4f core levels of ReO_3 films. XPS spectra for samples with the incremental deposition of NPB on ITO/high EA material (1 nm) substrates. (a) Mo 3d core levels of MoO_3 film and (b) Re 4f core levels of ReO_3 film.

between Mo^{VI} and Mo^V is 43% : 57% in the case of MoO_3/NPB (3 nm), as shown in Fig. S4b. The higher ratio of Mo^V species compared to the case of pristine 1 nm thick MoO_3 film is due to the reduction of MoO_3 by NPB molecules.

A little different results are observed for ReO_3 (Fig. 5b). The spectrum of 1 nm thick ReO_3 film before NPB deposition shows mainly a single Re $4f_{5/2}$ and $4f_{7/2}$ doublet with only small portion of a pair of shoulder peaks. The binding energies of the Re $4f_{5/2}$ and $4f_{7/2}$ doublet are 48.3 eV and 46.0 eV, respectively, which are close to the reported values[31]. The pair of shoulder peaks is located at 45.6 eV and 43.1 eV, respectively, by Gaussian curve fitting as shown in Fig. S4c. These shoulder peaks are reduced forms of Re such as Re^{IV} species[31], indicating generation of gap state close to the Fermi level similar to the case of pristine 1 nm thick MoO_3 film. The deposition of NPB on the ReO_3 film increased the portion of the shoulder peaks at a lower binding energy level, indicating generation of Re^{IV} species. The ratio between Re^{VI} and Re^{IV} is 55% : 45% in the case of ReO_3/NPB (4 nm), as shown in Fig. S4d, increased from 86% : 14% in the pristine 1 nm thick ReO_3 film (Fig. S4c). The higher ratio of Re^{IV} species compared to the case of the pristine 1 nm thick ReO_3 film is also due to the reduction of ReO_3 film by NPB molecules. These reductions in the oxidation states of MoO_3 and ReO_3 reflect positive charge transfer to NPB and a *p*-type doping effect in the NPB matrix, consistent with the large negative vacuum level shifts in the UPS spectra[30]. It is interesting to note that the portion of the formation of the reduced form of ReO_3 by the deposition of NPB is higher than MoO_3. Moreover the reduction is divalent (Re^{IV}) for ReO_3 compared to

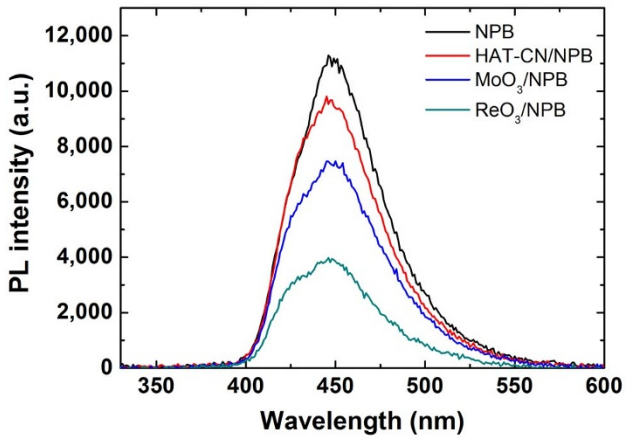

Figure 6 | PL intensities of 50 nm thick NPB films with and without high EA materials as a function of wavelength.

the monovalent (Mo^{V}) for MoO_3. These facts indicate that more charge-transfer complexes are formed at the ReO_3/NPB interface than the MoO_3/NPB interface.

More evidence of the formation of the charge-transfer complex can be obtained from PL experiment of the high EA material/NPB layers deposited on quartz substrate[12]. The PL intensities of 50 nm thick NPB films with and without high EA materials are displayed in Fig. 6 as a function of wavelength. The PL intensities decreased significantly when high EA materials were inserted between the quartz glass and the NPB film compared with that of the NPB-only film on quartz glass. The PL efficiency of the NPB film without an interlayer was 30.23%, whereas the PL efficiencies of the NPB films on HAT-CN, MoO_3, and ReO_3 interlayers were 28.42%, 22.24%, and 11.34%, respectively. These results indicate that not only charge-transfer complexes are formed at the high EA materials/NPB interfaces, because charge-transfer complexes near the interfaces behave as quenching sites for excitons in the NPB films through polaron–exciton quenching[32–34]; also, the degrees of formation of charge-transfer complexes are different for different high EA materials. Among the interlayers, ReO_3 gives the highest density of charge-transfer complexes, followed by MoO_3 and HAT-CN. These charge-transfer complexes at the high EA materials/NPB interfaces can be easily dissociated to free carriers by an applied electric field or thermal energy, because the ionization energies of hole carriers in *p*-type-doped systems are small (approximately 10–20 meV)[35]. These hole carriers generated from charge-transfer complexes at the interface can be injected into the NPB matrix without overcoming the hole injection barrier. The formation of a perfect ohmic contact is therefore achieved not only as a result of the low hole injection barrier, which is consistent with the polaron energy of the organic layer, but also because of the high degree of charge generation at the interface.

Discussion

In conclusion, we demonstrated the formation of a perfect ohmic contact at an ITO/NPB interface, using ReO_3 as an interfacial layer. The hole injection efficiency was close to 100% at the interface, which was much higher than those achieved using interfacial layers of HAT-CN and MoO_3. Interestingly, UPS measurements showed that ReO_3 and MoO_3 interfacial layers resulted in similar hole injection barriers of ≈0.4 eV to NPB, indicating that the Fermi level is pinned to the polaron energy level of NPB, even though hole injection with the ReO_3 interlayer is superior to that with the MoO_3 interlayer. This contradiction was resolved based on the differences among the degrees of charge generation in the NPB layers near the interfaces for different high EA materials, observed by XPS and PL intensity measurements. Among the interlayers, ReO_3 gave the highest degree of formation of charge-transfer complexes, followed by MoO_3 and HAT-CN. The formation of a perfect ohmic contact by the ReO_3 layer is therefore achieved not only as a result of a low hole injection barrier, which is consistent with the polaron energy of the organic layer, but also because of the high degree of charge generation at the interface. The development of the perfect ohmic contact between ITO and OSs will contribute to improve the performance of the organic optoelectronic devices utilizing the transparent electrodes by removing the parasitic resistance.

Methods

Fabrication and characterization of hole-only devices. High EA materials, namely HAT-CN, MoO_3, and ReO_3, were selected as the interfacial layer and NPB was selected as the hole-transporting organic semiconductor. Hole-only devices were fabricated by thermal evaporation in a high vacuum (≈10^{-5} Pa). Prior to deposition, the ITO substrates were cleaned with ultrapurified water, acetone, and isopropyl alcohol, and then dried in an oven at 80°C. We used hole-only devices with the structure glass/ITO (150 nm)/high EA material (1 nm)/NPB (1,000 nm)/high EA material (1 nm)/Ag (70 nm) to measure the *J–F* characteristics. The high EA materials and NPB were thermally evaporated at rates of 0.05 Å/s and 2.0 Å/s, respectively. A hole-only device with the structure glass/ITO (150 nm)/NPB (1,850 nm)/Ag (70 nm) was fabricated using the same procedure, and the hole mobility was measured using the time-of-flight method. All the devices were encapsulated immediately after deposition in a nitrogen atmosphere, using an epoxy glue and cavity glass lids. The active area of each device was 2 mm × 2 mm. The *J–F* characteristics of the hole-only devices were measured using a Keithley 237 semiconductor parameter analyser. For the time-of-flight measurements, a nitrogen laser (337 nm) (KEC-150, USHO optical system) was used to generate electron–hole pairs. A dc power supply was used to provide the bias voltage for hole detection. A digital oscilloscope (TDS3052B, Tektronix) was used to capture the voltage across a current-sensing resistor, which was connected in series to the samples. All *J–F* or time-of-flight measurements were performed in an ambient atmosphere.

Photoemission spectroscopy analysis. Experiments were carried out in two interconnected ultrahigh-vacuum chambers, one for thin film deposition and the other for spectroscopic analysis, with a base pressure of the order of 10^{-7} Pa. The UPS valence band spectra were measured using He Iα (21.2 eV) as the excitation source. XPS core level spectra were measured using Al Kα (1,486.6 eV) photon lines. The UPS and XPS resolutions were 0.15 and 0.5 eV, respectively. The detailed experimental procedures have been described in previous reports[36,37].

PL measurements. PL spectra of the studied films were measured using an integrating sphere. A continuous wave He/Cd laser (325 nm) (Series 56, Omnichrome) was used as the excitation light source and a monochromator attached to a photomultiplier tube was used as the optical detector system. NPB films of thickness 50 nm were thermally evaporated on clean quartz glass/high EA material layer (1 nm) substrates.

1. Nüesch, F., Forsythe, E. W., Le, Q. T., Gao, Y. & Rothberg, L. J. Importance of indium tin oxide surface acido basicity for charge injection into organic materials based light emitting diodes. *J. Appl. Phys.* **87**, 7973–7980 (2000).
2. Helander, M. G. *et al.* Chlorinated indium tin oxide electrodes with high work function for organic device compatibility. *Science* **332**, 944–947 (2011).
3. Arias, A. C., Granström, M., Petritsch, K. & Friend, R. H. Organic photodiodes using polymeric anodes. *Synth. Met.* **102**, 953–954 (1999).
4. Kim, W. H. *et al.* Molecular organic light-emitting diodes using highly conducting polymers as anodes. *Appl. Phys. Lett.* **80**, 3844–3846 (2002).
5. Yoo, S.-J., Lee, J.-H., Lee, J.-H. & Kim, J.-J. Doping-concentration-dependent hole mobility in a ReO_3 doped organic semiconductor of 4,4′,4″-tris(*N*-(2-naphthyl)-*N*-phenyl-amino)-triphenylamine. *Appl. Phys. Lett.* **102**, 183301 (2013).
6. Leem, D.-S. *et al.* Low driving voltage and high stability organic light-emitting diodes with rhenium oxide-doped hole transporting layer. *Appl. Phys. Lett.* **91**, 011113 (2007).
7. Lee, J.-H., Leem, D.-S., Kim, H.-J. & Kim, J.-J. Effectiveness of *p*-dopants in an organic hole transporting material. *Appl. Phys. Lett.* **94**, 123306 (2009).
8. Lee, J.-H., Leem, D.-S. & Kim, J.-J. High performance top-emitting organic light-emitting diodes with copper iodide-doped hole injection layer. *Org. Electron.* **9**, 805–808 (2008).
9. Cheung, C. H., Song, W. J. & So, S. K. Role of air exposure in the improvement of injection efficiency of transition metal oxide/organic contact. *Org. Electron.* **11**, 89–94 (2010).
10. Small, C. E., Tsang, S.-W., Kido, J., So, S. K. & So, F. Origin of enhanced hole injection in inverted organic devices with electron accepting interlayer. *Adv. Funct. Mater.* **22**, 3261–3266 (2012).
11. Matsushima, T., Kinoshita, Y. & Murata, H. Formation of ohmic hole injection by inserting an ultrathin layer of molybdenum trioxide between indium tin oxide and organic hole-transporting layers. *Appl. Phys. Lett.* **91**, 253504 (2007).

12. Matsushima, T. & Murata, H. Observation of space-charge-limited current due to charge generation at interface of molybdenum dioxide and organic layer. *Appl. Phys. Lett.* **95**, 203306 (2009).
13. Wang, Z. B., Helander, M. G., Greiner, M. T., Qiu, J. & Lu, Z. H. Analysis of charge-injection characteristics at electrode-organic interface: case study of transition-metal oxides. *Phys. Rev. B.* **80**, 235325 (2009).
14. Kröger, M. *et al.* Role of the deep-lying electronic states of MoO_3 in the enhancement of hole-injection in organic thin films. *Appl. Phys. Lett.* **95**, 123301 (2009).
15. Shen, Y., Hosseini, A. R., Wong, M. H. & Malliaras, G. G. How to make ohmic contacts to organic semiconductors. *ChemPhysChem* **5**, 16–25 (2004).
16. Lee, J.-H., Leem, D.-S. & Kim, J.-J. Effect of host organic semiconductors on electrical doping. *Org. Electron.* **11**, 486–489 (2010).
17. Lambert, M. A. & Mark, P. *Current Injection in Solids* Academic Press: New York and London (1970).
18. Murgatroyd, P. N. Theory of space-charge-limited current enhanced by Frenkel effect. *J. Phys. D: Appl. Phys.* **3**, 151–156 (1970).
19. So, S. K., Tse, S. C. & Tong, K. L. Charge transport and injection to phenylamine-based hole transporters for OLEDs applications. *J. Display Technol.* **3**, 225–232 (2007).
20. Tsang, S. W., Denhoff, M. W., Tao, Y. & Lu, Z. H. Charge-carrier induced barrier-height reduction at organic heterojunction. *Phys. Rev. B.* **78**, 081301(R) (2008).
21. Lee, S. *et al.* Determination of the interface energy level alignment of a doped organic hetero-junction using capacitance-voltage measurements. *Org. Electron.* **13**, 2346–2351 (2012).
22. Greiner, M. T. *et al.* Universal energy-level alignment of molecules on metal oxides. *Nat. Mater.* **11**, 76–81 (2012).
23. Ishii, H., Sugiyama, K., Ito, E. & Seki, K. Energy level alignment and interfacial electronic structures at organic/metal and organic/organic interfaces. *Adv. Mater.* **11**, 605–625 (1999).
24. Lee, H. *et al.* The origin of the hole injection improvements at indium tin oxide/molybdenum trioxide/*N*,*N*′-bis(1-naphthyl)-*N*,*N*′-diphenyl-1,1′-biphenyl-4,4′-diamine interfaces. *Appl. Phys. Lett.* **93**, 043308 (2008).
25. Braun, S., Osikowicz, W., Wang, Y. & Salaneck, W. R. Energy level alignment regimes at hybrid organic-organic and inorganic-organic interfaces. *Org. Electron.* **8**, 14–20 (2007).
26. Braun, S., Salaneck, W. R. & Fahlman, M. Energy-level alignment at organic/metal and organic/organic interfaces. *Adv. Mater.* **21**, 1450–1472 (2009).
27. Werfel, F. & Minni, E. Photoemission study of the electronic structure of Mo and Mo oxides. *J. Phys. C: Solid State Phys.* **16**, 6091–6100 (1983).
28. Bhosle, V., Tiwari, A. & Narayan, J. Epitaxial growth and properties of MoO_x ($2 < x < 2.75$) films. *J. Appl. Phys.* **97**, 083539 (2005).
29. Kanai, K. *et al.* Electronic structure of anode interface with molybdenum oxide buffer layer. *Org. Electron.* **11**, 188–194 (2010).
30. Wu, C.-I. *et al.* Electronic and chemical properties of molybdenum oxide doped hole injection layers in organic light emitting diodes. *J. Appl. Phys.* **105**, 033717 (2009).
31. Luo, J., Xiao, L., Chen, Z., Qu, B. & Gong, Q. ReO_x charge injection/blocking layers in organic electronic devices. *J. Phys D: Appl. Phys.* **43**, 385101 (2010).
32. Matsushima, T. *et al.* Interfacial charge transfer and charge generation in organic electronic devices. *Org. Electron.* **12**, 520–528 (2011).
33. Mo, H.-W. *et al.* Infrared organic photovoltaic device based on charge transfer interaction between organic materials. *Org. Electron.* **14**, 291–294 (2013).
34. Ng, T.-W., Lo, M.-F., Yang, Q.-D., Fung, M.-K. & Lee, C.-S. Near-infrared electric power generation through sub-energy-gap absorption in an organic-inorganic composite. *Adv. Funct. Mater.* **22**, 3035–3042 (2012).
35. Tietze, M. L., Burtone, L., Riede, M., Lüssem, B. & Leo, K. Fermi level shift and doping efficiency in *p*-doped small molecule organic semiconductors: a photoelectron spectroscopy and theoretical study. *Phys. Rev. B.* **86**, 035320 (2012).
36. Wu, C.-I., Lee, G.-R. & Pi, T.-W. Energy structures and chemical reactions at the Al/LiF/Alq_3 interfaces studied by synchrotron-radiation photoemission spectroscopy. *Appl. Phys. Lett.* **87**, 212108 (2005).
37. Wu, C.-I. *et al.* Electronic structures and electron-injection mechanisms of cesium-carbonate-incorporated cathode structures for organic light-emitting devices. *Appl. Phys. Lett.* **88**, 152104 (2006).

Acknowledgments

This work was supported by a New & Renewable Energy Technology Development Program of the Korea Institute of Energy Technology Evaluation and Planning (KETEP) grant, funded by the Korea government Ministry of Knowledge Economy (No. 20113020010070) and under the framework of international cooperation program managed by National Research Foundation of Korea (2012K2A1A2033115).

Author contributions

S.-J.Y. mainly designed the experimental concept and analysed most of the data, and wrote the manuscript. J.-H.C. performed the photoemission spectroscopic analysis (UPS and XPS data). S.-J.Y. and J.-H.L. together interpreted the hole injection properties from the *J–F* characteristics of hole-only devices. C.-K.M. performed the PL quantum yield measurements. C.-I.W. analysed the UPS and XPS data. J.-J.K. supervised and motivated this work and co-wrote the manuscript. All authors discussed the results and contributed to this paper.

Additional information

Supplementary information accompanies this paper at http://www.nature.com/scientificreports

Competing financial interests: The authors declare no competing financial interests.

How to cite this article: Yoo, S.-J. *et al.* Formation of perfect ohmic contact at indium tin oxide/*N*,*N*′-di(naphthalene-1-yl)-*N*,*N*′-diphenyl-benzidine interface using ReO_3. *Sci. Rep.* **4**, 3902; DOI:10.1038/srep03902 (2014).